A three-dimensional finite element simulation for transport of nuclear waste contaminationin porous media

R.E. Ewing
Texas A&M University, College Station, Texas

H. Wang
University of South Carolina, Columbia, South Carolina

M.A. Celia
Princeton University, Princeton, New Jersey

R.C. Sharpley
University of South Carolina, Columbia, South Carolina

ABSTRACT: Model equations for transport of nuclear-waste contamination in three-dimensional porous media are presented with a description of linearization techniques based up on the inherent physics. A three-dimensional finite element method for nuclear waste contamination involving the transport of fluid, heat, brine, and trace-species radionuclides by logically rectangular hexahedral elements are discussed.

1 INTRODUCTION

The growing incidence of contamination of groundwater by high-level nuclear waste and a wide variety of other sources makes a proper description and understanding of contaminant transport in porous media very important. A model was developed for use by the Nuclear Regulatory Commission for the analysis of deep geologic nuclear waste disposal facilities, which involves a fully transient coupled system of equations for transport of total fluid, heat, brine, and trace-species radionuclides. The equations used here are obtained by combining appropriate continuity and constitutive relations and have been derived by several authors (Aziz and Settari (1979), Bear (1979), Cooper (1966), Reeves and Cranwell (1981), and Reeves, Ward, Johns, and Cranwell (1986)). The resulting relations for the total fluid, heat, brine, and the ith component of radionuclides may be stated as follows:

$$-\nabla \cdot \underline{u} - q + R'_s = 0, \tag{1}$$

$$\begin{aligned} -\nabla \cdot (H\underline{u}) + \nabla \cdot (\mathrm{E}_H \nabla T) - q_L - qH - q_H \\ = [\phi c_p + (1-\phi)\bar{\rho}_R c_{pR}] \frac{\partial T}{\partial t}, \end{aligned} \tag{2}$$

$$-\nabla \cdot (\hat{c}\underline{u}) + \nabla \cdot (\mathrm{E}_c \nabla \hat{c}) - q\hat{c} - q_c + R_s = \phi \frac{\partial \hat{c}}{\partial t}, \tag{3}$$

$$\begin{aligned} \nabla \cdot (c_i \underline{u}) + \nabla \cdot (\mathrm{E}_c \nabla c_i) - qc_i - q_{c_i} + q_{0i} \\ + \sum_{j=1}^{N} k_{ij}\lambda_j K_j \phi c_j - \lambda_i K_i \phi c_i \\ = \phi K_i \frac{\partial c_i}{\partial t}, \qquad i = 1, 2, \ldots, N. \end{aligned} \tag{4}$$

The quantity $\underline{u} = (u_1, u_2, u_3)$ is the Darcy velocity of the total fluid, $\hat{c}$ is the concentration of the dominant species (brine in our case), c_i ($i = 1, 2, \ldots, N$) is the concentration of the ith component of trace-species (radionuclides in our case), T is the temperature, $q = q(\underline{x}, t)$ is a production term, $R'_s = R'_s(\hat{c}) = \frac{c_s \phi k_s f_s}{1+c_s}(1-\hat{c})$ is a salt-dissolution term for the fluid equation, $q_L = q_L(T)$ is a heat loss to the under/overburden term, qH is an injected enthalpy term, $q_H = q_H(T)$ is a produced enthalpy term, $q\hat{c}$ is an injected brine term, $q_c = q_c(\hat{c})$ is a produced brine term, $R_s = R_s(\hat{c}) = \phi k_s f_s (1-\hat{c})$ is a salt-dissolution term for the brine equation, qc_i are injected components terms, $q_{c_i} = q_{c_i}(c_i)$ are produced components terms, $q_{0i} = q_{0i}(c_i)$ are waste leach terms, ϕ is the porosity of the medium, ρ_R is the density, k_{ij} and K_j describe distribution coefficients and the retardation factor for each component, $\sum_{j=1}^{N} k_{ij}\lambda_j K_j \phi c_j$ describe generation of component i by decay of j, and $\lambda_i K_i \phi c_i$ is the decay for component i.

Several quantities in equations (1)–(4) require further definition in terms of the basic parameters. The tensors in equations (2)–(4) are defined as sums of dispersion and molecular terms:

$$\mathrm{E}_c = \mathrm{D} + D_m \mathrm{I} \tag{5}$$

and

$$\mathrm{E}_H = \mathrm{D}c_{pw} + K_m \mathrm{I}, \tag{6}$$

where

$$D_{ij} = \alpha_T |\underline{u}| \delta_{ij} + (\alpha_L - \alpha_T) u_i u_j / |\underline{u}| \tag{7}$$

in a cartesian system. α_L and α_T are the coefficients of longitudinal and transverse dispersions, D_m and K_m are the molecular diffusion coefficients. The nonlinearities in the dispersion terms significantly complicate the related computational schemes. The tensor form requires a twenty-seven-point communication star in three dimensions.

Also, absorption of radionuclides is included via an assumption of a linear equilibrium isotherm. This yields the distribution coefficient k_{di} and the retardation factor for each component

$$K_i = 1 + \rho_R k_{di}(1-\phi)/\phi. \tag{8}$$

Equations (1)–(4) are coupled by a mixing rule for viscosity, $\mu = \mu(\hat{c})$, and three auxiliary relations for Darcy flux, fluid enthalpy and fluid internal energy are given, respectively, by

$$\underline{u} = -\frac{\mathrm{k}}{\mu}\left(\nabla p - \rho_0 \frac{g}{g_c}\nabla z\right), \tag{9}$$

$$H = U_0 + U + p/\rho_0, \tag{10}$$

$$U = c_p(T - T_0), \tag{11}$$

where $U_0 = U_0(\underline{x})$, $T_0 = T(\underline{x}, 0)$, p is the pressure, k is the permeability of the medium, ρ_0 is the density of the fluid.

In the system above, our primary unknowns are the pressure p, the Darcy velocity $\underline{u}$, the concentration $\hat{c}$ of the dominant species, the concentrations c_i $(i = 1, 2, \ldots, N)$ of the trace-species, and the temperature T. In addition to the equations above, the initial and boundary conditions must be given to close the system.

2 LINEARIZATION TECHNIQUES

The system (1)–(11) presented in Section 1 is a large coupled system of strongly nonlinear partial differential equations. The combination of strong nonlinearities and close couplings between the equations cause difficulties in solving the system. Due to the enormous size of the applications, these equations cannot be solved in a fully-coupled, fully-implicit fashion. Thus, some linearization techniques must be used to obtain the numerical solution. However, a blind linearization with little regard to the properties of the equations or the solutions can result in extremely large, ill-conditioned, nonlinear systems; the accurate solution of these equations can be extremely difficult and expensive. Choices of implicitness and decoupling of the equations are forms of linearization and must be analyzed and treated with great care for these difficult problems.

Before we describe our linearization techniques here, let us briefly discuss the system (1)–(11). equations (1) and (9) define the pressure p and the Darcy velocity $\underline{u}$. Nevertheless, the coefficient $\mu(\hat{c})$ in (9) depends on the $\hat{c}$ defined by equation (3). In this manner, equations (1) and (9) are coupled to equation (3). On the other hand, equation (3) is coupled to equations (1) and (9) through the Darcy velocity $\underline{u}$. Also, equations (2) and (4) are coupled to equations (1) and (9) through the Darcy velocity $\underline{u}$. But c_i $(i = 1, 2, \ldots, N)$ do not affect the viscosity μ in equation (9) and so do not affect the Darcy velocity $\underline{u}$.

Based on these observations, we now present our linearization techniques. Since the system (1)–(11) is time-dependent, we utilize an IMPES-type (implicit pressure and explicit saturation) modified-Picard time marching algorithm to solve the system (1)–(11) for the unknowns p, $\underline{u}$, $\hat{c}$, c_i, and T. Assume that we know $\hat{c}(\underline{x}, t^n)$ and $c_i(\underline{x}, t^n)$ (which are the initial conditions for the system (1)–(11) when $n = 0$), we solve for $p(\underline{x}, t^n)$, $\underline{u}(\underline{x}, t^n)$, $\hat{c}(\underline{x}, t^{n+1})$, $c_i(\underline{x}, t^{n+1})$ and $T(\underline{x}, t^{n+1})$ by the following procedure

STEP 1. Solve for the pressure $p(\underline{x}, t^n)$, the Darcy velocity $\underline{u}(\underline{x}, t^n)$ and the concentration of the brine $\hat{c}(\underline{x}, t^{n+1})$.

(i) We solve for the pressure $p(\underline{x}, t^n)$ and the Darcy velocity $\underline{u}(\underline{x}, t^n)$ implicitly (the 'IMP' in IMPES). Substituting equation (9) into equation (1), we obtain a second-order elliptic equation for the pressure p

$$-\nabla \cdot \left(\frac{\mathrm{k}}{\mu}\left(\nabla p - \rho_0 \frac{g}{g_c}\nabla z\right)\right) = -q + R'_s. \tag{12}$$

We take $\hat{c}$ in $\mu(\hat{c})$ of equation (12) to be $\hat{c}(\underline{x}, t^n)$ and solve equation (12) for the pressure $p(\underline{x}, t^n)$ by finite element methods.

(ii) We substitute the pressure $p(\underline{x}, t^n)$ into equation (9) to compute the Darcy velocity $\underline{u}(\underline{x}, t^n)$.

(iii) We solve equation (3) for the concentration $\hat{c}(\underline{x}, t^{n+1})$ of the brine explicitly (the 'ES' in IMPES). Namely, we approximate $\underline{u}$ in equation (3) by $\underline{u}(\underline{x}, t^n)$ and solve equation (3) for $\hat{c}(\underline{x}, t^{n+1})$ by finite element methods. Here ES in IMPES refers to the fact that we have used

$\underline{u}(\underline{x}, t^n)$ to approximate $\underline{u}$ explicitly, no matter the numerical scheme for equation (3) is an explicit scheme and an implicit scheme.

(iv) If the solutions $p(\underline{x}, t^n)$, $\underline{u}(\underline{x}, t^n)$ and $\hat{c}(\underline{x}, t^{n+1})$ are accurate enough, we will directly go to Step 3 to solve the transport equations (4) for the trace-species and the temperature equation (2). Otherwise, we will perform iterations on equations (3) and (12) as described below in Step 2.

STEP 2. As mentioned before, if the solutions $p(\underline{x}, t^n)$, $\underline{u}(\underline{x}, t^n)$ and $\hat{c}(\underline{x}, t^{n+1})$ are not accurate enough, we will perform iterations on equations (3) and (12) according to the following procedure:

(i) We choose $p^{(0)}(\underline{x}, t^{n+1})$ to be $p(\underline{x}, t^n)$, $\underline{u}^{(0)}(\underline{x}, t^{n+1})$ to be $\underline{u}(\underline{x}, t^n)$ and $\hat{c}^{(1)}(\underline{x}, t^{n+1})$ to be $\hat{c}(\underline{x}, t^{n+1})$ obtained in Step 1.

(ii) For iteration parameter $l = 1, \ldots$, we take $\hat{c}$ in $\mu(\hat{c})$ of equation (12) to be $\hat{c}^{(l)}(\underline{x}, t^{n+1})$, then repeat the (i) and (ii) in Step 1 to obtain $p^{(l)}(\underline{x}, t^{n+1})$ and $\underline{u}^{(l)}(\underline{x}, t^{n+1})$.

(iii) Replacing $\underline{u}$ in equation (3) by $\underline{u}^{(l)}(\underline{x}, t^n)$, we repeat (iii) in Step 1 and obtain $\hat{c}^{(l+1)}(\underline{x}, t^{n+1})$.

(iv) If the numerical solutions obtained are not accurate enough, go back to (i) within this Step with l replaced by $l+1$. Otherwise, go to Step 3 for the solutions of transport equations (4) for the trace species and for the solutions of temperature equation (2).

In summary, by utilizing the intrinsic physics of the system (1)–(11), we have successfully decoupled the system. Namely, we first solve equations (3) and (12) iteratively to obtain satisfactory approximations to p, $\underline{u}$ and $\hat{c}$. If no iterations are involved, then Step 1 yields the numerical solutions $p(\underline{x}, t^n)$, $\underline{u}(\underline{x}, t^n)$ and $\hat{c}(\underline{x}, t^{n+1})$. If iterations are involved, then Step 2 yields the mth iterative solutions $p^{(m)}(\underline{x}, t^{n+1})$, $\underline{u}^{(m)}(\underline{x}, t^n)$ and the $(m+1)$th iterative solution $\hat{c}^{(m+1)}(\underline{x}, t^{n+1})$ in addition to $p(\underline{x}, t^n)$ and $\underline{u}(\underline{x}, t^n)$ generated in Step 1. Here m is the number of iterations performed in the current time t^{n+1}.

After we obtain the approximations p, $\underline{u}$ and $\hat{c}$, we are now in a position to solve equations (4) for the concentrations $c_i(\underline{x}, t^{n+1})$ $(i = 1, 2, \ldots, N)$ of the trace species and to solve equation (2) for the temperature T. Note that equations (4) are coupled together for all c_i through the reaction terms (the next to the last term on the left-hand side of the equations), we solve equations (4) iteratively as follows

STEP 3. Solve equations (4) for the concentrations c_i $(i = 1, 2, \ldots, N)$ of the trace species and equation (2) for the temperature T.

(i) Choose $c_i^{(0)}(\underline{x}, t^{n+1})$ to be $c_i(\underline{x}, t^n)$ for $i = 1, 2, \ldots, N$.

(ii) For iteration parameter $l = 0, 1, \ldots$, we approximate c_i in $q_{c_i}(c_i)$ and $q_{0i}(c_i)$ in the ith equation of equations (4) by $c_i^{(l)}(\underline{x}, t^{n+1})$, and approximate c_j in $\sum_{j=1}^{N} k_{ij}\lambda_j K_j \phi c_j$ in the ith equation of equations (4) by $c_j^{(l)}(\underline{x}, t^{n+1})$ for $j = 1, 2, \ldots, N$ and $j \neq i$.

(iii) Each equation in equations (4) is reduced to linear variable-coefficient equation. Then we solve these N individual equations for $c_i^{(l+1)}(\underline{x}, t^{n+1})$ $(i = 1, 2, \ldots, N)$.

(iv) If $c_i^{(l+1)}(\underline{x}, t^{n+1})$ $(i = 1, 2, \ldots, N)$ are accurate enough, stop. Otherwise, go back to (ii) within this step with l replaced by $l + 1$.

(v) Choose $T^{(0)}(\underline{x}, t^{n+1})$ to be $T(\underline{x}, t^n)$. For iteration parameter $l = 0, 1, \ldots$, we approximate T in $q_L(T)$ and $q_H(T)$ in equation (2) by $T^{(l)}(\underline{x}, t^{n+1})$. Then we solve equation (2) for the temperature $T^{(l+1)}(\underline{x}, t^{n+1})$. If $T^{(l+1)}(\underline{x}, t^{n+1})$ is accurate enough, stop. Otherwise, repeat this process with l replaced by $l + 1$.

When we decoupled equation (4) in (ii)–(iii) in Step 3, we adopt a Jacobi approach to update the reaction terms. The Jacobian approach is fully parallelizable in that all the N equations in equations (4) can be solved independent of one another. This is especially important when many trace species are involved, i.e, when N is large. However, the Jacobi approach usually converges more slowly than the Gauss-Seidel approach. Thus, we can also adopt a Gauss-Seidel approach. Namely, we replace (ii)–(iii) in Step 3 by (ii')–(iii') below.

(ii') For iteration parameter $l = 0, 1, \ldots$, we solve each individual equation in equations (4) sequentially. When we solve the ith equation $(i = 1, 2, \ldots, N)$ in equations (4) for $c_i^{(l+1)}(\underline{x}, t^{n+1})$, we approximate c_i in $q_{c_i}(c_i)$ and $q_{0i}(c_i)$ by $c_i^{(l)}(\underline{x}, t^{n+1})$, approximate c_j in $\sum_{j=1}^{N} k_{ij}\lambda_j K_j \phi c_j$ by $c_j^{(l+1)}(\underline{x}, t^{n+1})$ for $j < i$,

and approximate c_j in $\sum_{j=1}^{N} k_{ij}\lambda_j K_j \phi c_j$ by $c_j^{(l)}(\underline{x}, t^{n+1})$ for $j > i$.

(iii') Then the ith equation in equations (4) is reduced to a linear variable-coefficient equation. We solve this equation for $c_i^{(l+1)}(\underline{x}, t^{n+1})$ $(i = 1, 2, \ldots, N)$.

When we solve equations (2)–(4), if the Courant number is larger than 1, we will subdivide the time step Δt into local time steps Δt_{lc} such that the Courant number with local time step Δt_{lc} will be less than 1. Then we can apply the above procedure Steps 1–3 to solve the system (1)–(11) over the refined the time steps.

As mentioned above, the Gauss-Seidel approach converges faster than the Jacobi, but it has the drawback each equation in equations (4) must be solved in sequential order. On the other hand, the Gauss-Seidel approach uses less storage than the Jacobi. In practical applications, we should choose the appropriate approach based on the physical problems and the available computational resources.

3 NUMERICAL METHODS AND THEIR IMPLEMENTATION

Previously, simulators have been developed for numerical simulations to the system (1)–(11) defined over three-dimensional rectangular domains, but using orthogonal grids or "bricks". Due to the complicated subsurface geology and the heterogeneity of the media through which the contaminants are transported, the system (1)–(11) is usually modeled over polyhedral domains. In fact, in many real field applications the domains can be rectangular in the x, y directions, but with different depths in the z direction for different x, y pairs where $\underline{x} = (x, y, z)$. While the use of tetrahedral partitions is a general approach to solving equations (1)–(4), tetrahedral partitions generate very complicated data structure and make the coding very difficult to implement. In our simulations, we use three-dimensional logically rectangular partitions, i.e., hexahedral partitions. More precisely, we use rectangular partitions in the x, y plane and use the same number of nodal points along the z direction for every nodal point x, y on the x, y plane. In this way, we obtain a hexahedral partition. Even though the original domain is not a rectangular domain and our partition is not a three-dimensional rectangular partition, our partition still maintains the same data structure as a rectangular domain with a rectangular partition, so the algorithms can be implemented more easily.

Moreover, the code can easily take element-by-element input for various parameters, and thus is able to simulate the contaminant transport in heterogeneous media, permitting the flexibility to carry out real field simulations.

As mentioned in Section 2, the transport equations (2)–(4) are solved by using a lumped finite element approximation, with upstream weighting as an option. The pressure equation (12) is solved by using the finite element method. In the code, material within each element is assumed to be homogeneous, but different material properties can be assigned to different elements.

The matrix that results from the finite element approximation of equation (1) is symmetric and positive definite. Therefore, standard preconditioned conjugate gradient methods work well in inverting the matrix equation. For this work, a simple diagonal preconditioning is used due to the ease of parallel implementation. For the transport equations (2)–(4), the resulting matrices are not symmetric. Because the preconditioned conjugate gradient methods are guaranteed to converge for symmetric matrices only, conjugate gradient squared methods are used to solve the matrix equations from the transport equations (2)–(4).

4 NUMERICAL EXPERIMENTS

In this section, we perform some numerical experiments to simulate the contaminant transport. In these simulations, the spatial domain is rectangular in x and y directions. The length is 4000 meters and the width is 4000 meters. Due to the complicated subsurface geology, the spatial domain has different depth in the z direction for different x, y pairs, varying from 30 meters to 200 meters. Since these simulations use some realistic data, the bottom surface is not given by a function in closed form and is in fact read from a table. The graph of the spatial domain is presented in Figure 1.a.

The initial concentrations are defined by a table and do not have a closed function form. Since this is a three dimensional simulation, we can only plot the isosurfaces for the concentrations. In figure 1.a. and 1.d., we present the initial isosurfaces for the concentration of the brine with the concentration levels 0.052 and 0.103, respectively.

In these simulations, we use a 127 by 137 nonuni-

form rectangular partition in the x, y plane. For each node in the x, y plane, we partition the depth into 11 elements uniformly. Since the bottom surface of the spatial domain is not flat (and in fact varies dramatically), the nodes in the z direction varies as the x, y pair varies. But the number of nodes in the z direction is fixed (12 in this simulation) and is independent of the x, y pairs. Notice that the top surface of the domain is planar (horizontal in this particular simulation) and the partition in the z direction is uniform, we naturally end up with a logically rectangular partition over the spatial domain of total 191,389 elements. Therefore, we have all the advantages of the logically rectangular partitions mentioned in Section 3. In particular, we maintain the data structure of rectangular partitions but we are able to simulate realistic contaminant transport over three-dimensional nonrectangular domains.

In our numerical simulations, we utilize our knowledge on the location of the initial plum of the concentration of the brine. Thus, we use fine meshes in both x and y directions over the region containing the plums and use coarse meshes over the region further away.

In our simulations, we simulated the contaminat transport for 400 days. We plotted the initial isosurface, the isosurface at 200 days, and the isosurface at 400 days for the concentration of the brine in Figures 1.a., 1.b., and 1.c., respectively. The concentration level used for these plots is 0.052. We also plot the corresponding isosurfaces for the concentration of the brine with the concentration level 0.103 in Figures 1.d., 1.e., and 1.f., respectively.

In these simulations, the regional fluid flow moves from the southeast corner of the illustrated domain to the northwest corner. The numerical results show that the contaminant is moving upstream to the regional flow, due to the significant effect of gravity. Since brine is the dominant species in these transport simulations, we have just presented the plots for the concentration of brine and have omitted the plots for pressure, Darcy velocity, concentrations of the trace-species and temperature for the sake of brevity.

5 DISCUSSION

In this paper, we describe a numerical method for the simulation of contaminant transport of radionuclides defined over a three-dimensional nonrectangular domain, which involves a fully transient coupled system of equations for transport of total fluid, heat, brine, and trace-species radionuclides. A finite element method over a logically rectangular partition of the domain is used. Numerical results are presented to demonstrate the strength of the method. For simplicity of the presentation, in this paper we only consider the special hexahedral domains which are rectangular in the x, y plane and are usually sufficient for many applications, it is straightforward to generalize the numerical methods to solve the system (1)–(11) on general hexahedral domains. We close by pointing out possible improvements regarding the methods presented in this paper.

In many cases, due to the strong heterogeneity of the subsurface geology, the media property $\mathbf{k}$ and $\hat{c}$-dependent μ are not smoothly distributed and may even have jumps. Consequently, the exact solution of equation (12) is not smooth and the numerical approximation p might not be accurate. If we substitue p into equation (9), we obtain the numerical Darcy velocity $\underline{u}$ by numerically differentiating p and then multiplying p by a rough coefficient $\mathbf{k}/\mu$. This leads to a numerical Darcy velocity $\underline{u}^h$ that might not be very accurate. Physically, while the pressure might not be smooth, the Darcy velocity usually is. Therefore, the mixed finite element method, which approximates the pressure and the Darcy velocity simultaneously, is expected to yield a more accurate numerical Darcy velocity. However, the mixed finite element method is usually more expensive to solve than standard finite element methods. While the mixed finite element method has been made more efficient when the permeability tensor $\mathbf{k}$ is a diagonal tensor and orthogonal meshes are used, additional research for mixed finite element method is needed when the permeability $\mathbf{k}$ is a full tensor or when logically rectangular meshes are used, especially for the three dimensional problems considered in this paper.

Because the transport equations (2)–(4) are strongly advection-dominated partial differential equations, the pure Eulerian finite element methods might yield numerical solutions with nonphysical oscillations or numerical dispersions. Moreover, the numerical iterations may converge very slowly, since the coefficient matrix is strongly nonsymmetric. Eulerian-Lagrangian methods, which take advantage of the flow, are more efficient but are more difficult to implement than the pure Eu-

lerian methods. Among the difficulties are the implementation of boundary conditions and the searching algorithms to follow characteristics that may consume a large portion of time for a general hexahedral partition. For Eulerian-Lagrangian techniques to address these problems see Celia, Russell, Herrera, and Ewing (1990), Ewing (1984), Ewing, Yuan, and Li (1989), and Ewing and Wang (1992).

ACKNOWLEDGEMENT

This research was supported in part by DOE, DE–AC05–840R21400, Martin Marietta, Subcontract, SK965C and SK966V, by NSF Grant Nos. DMS–8922865, and 8657419-CES, by funding from the Institute for Scientific Computation at Texas A&M University, and by funding from Office of Naval Research Contract No. 0014-88-K-0370.

REFERENCES

Aziz, H. & Settari, A. 1979. *Petroleum reservoir simulation.* Applied Science Publishers.

Bear, J. 1979. *Hydraulics of groundwater.* McGraw-Hill.

Bouloutas, E.T. 1992. *Improved methods of modeling flow and transport processes in partially saturated porous media.* Ph.D. Thesis, MIT, Department of Civil Engineering, Cambridge, MA.

Celia, M.A. & Binning, P. 1992, Multiphase models of unsaturated flow: Approaches to the governing equations and numerical methods. *Computational Methods in Water Resources* (Russell *et al.*, eds.): 257–272. Boston: Computational Mechanics Publications.

Celia, M.A., Russell, T.F., Herrera, I., & Ewing, R.E. 1990. An Eulerian-Lagrangian localized adjoint method for the advection-diffusion equation. *Advances in Water Resources* 13(4):187–206.

Cooper, H. 1966. The equation of ground-water flow in fixed and deforming coordinates. *J. Geophys. Res.* 71:4783–4790.

Ewing, R.E. (ed.). 1984. *Mathematics of reservoir simulation.* Frontiers in Applied Mathematics. Philadelphia: SIAM.

Ewing, R.E., Yuan, Y., and Li, G. 1989. Time stepping along characteristics for a mixed finite element approximation for compressible flow of contamination by nuclear waste in porous media. *SIAM J. Numer. Anal.* 26(6):1513–1524.

Ewing, R.E. and Wang, H. 1992. Eulerian-Lagrangian localized adjoint methods for reactive transport in groundwater. *IMA Preprint Series #1014.* University of Minnesota: Institute for Mathematics and Its Applications; *IMA Volume in Mathematics and Its Applications* (Wheeler *et al.*, eds.). Berlin: Springer-Verlag (to appear).

Hillel, D. 1980. *Fundamentals of soil physics.* New York: Academic Press.

Reeves, M. and Cranwell, R.M. 1981. User's manual for the Sandia waste-isolation flow and transport model (SWIFT) Release 4.81. *Sandia Report Nureg/CR–2324, SAND 81–2516, GR.*

Reeves, M., Ward, D.S., Johns, N.D., and Cranwell, R.M. 1986. Theory and implementation for the Sandia waste-isolution flow and transport model for fractured media (SWIFT) Release 4.84. *Sandia Report Nureg/CR–3328, SAND 83–1159, RW.*

Concentration Isosurfaces for Brine Solution

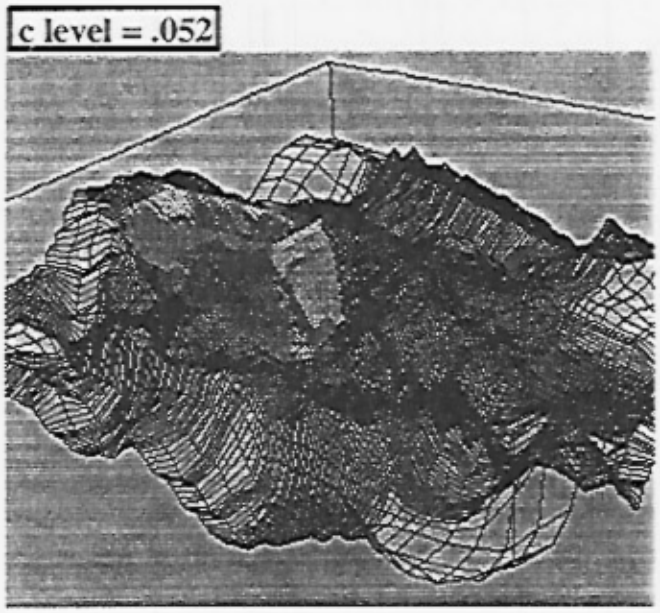

Fig.1.a : Initial Concentration

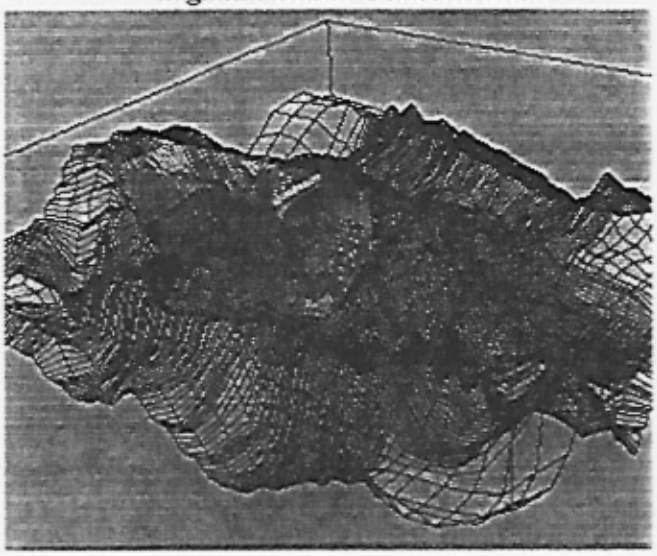

Fig. 1.b. Time = 200

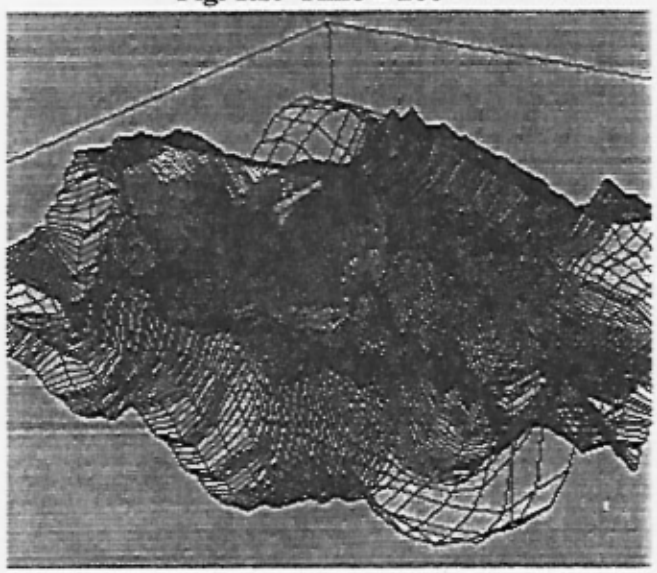

Fig. 1.c. Time = 400

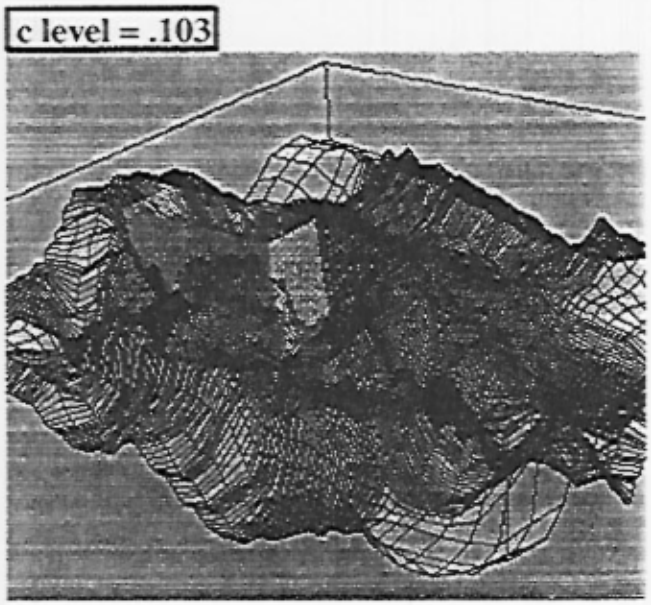

Fig. 1.d. Initial Concentration

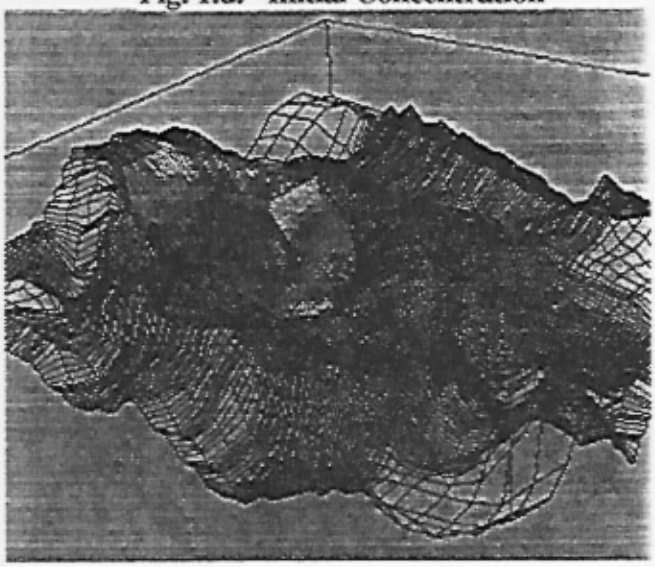

Fig.1.e. Time = 200

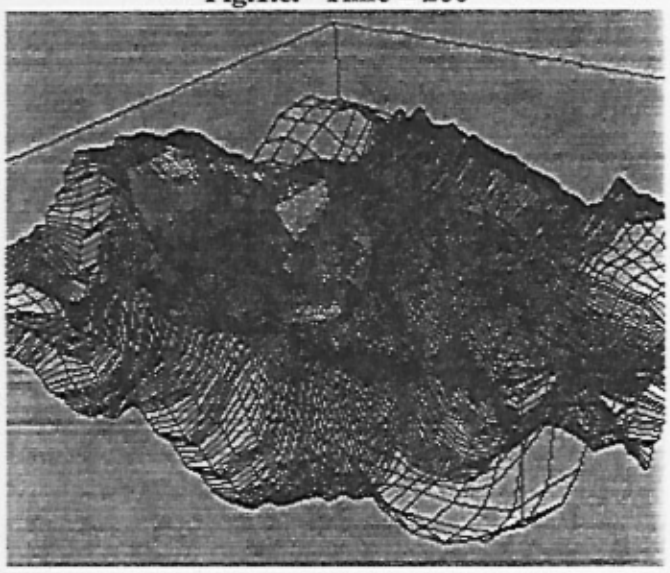

Fig.1.f. Time = 400

Figure 1